

Nanomechanical probing of thin-film dielectric elastomer transducers

Bekim Osmani, Saman Seifi, Harold S. Park, Vanessa Leung, Tino Töpfer, and Bert Müller

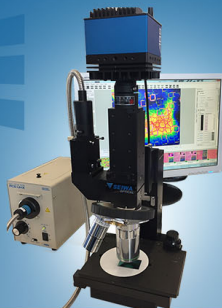
Citation: *Appl. Phys. Lett.* **111**, 093104 (2017); doi: 10.1063/1.5000736

View online: <http://dx.doi.org/10.1063/1.5000736>

View Table of Contents: <http://aip.scitation.org/toc/apl/111/9>

Published by the [American Institute of Physics](#)

The logo for SEIWA OPTICAL features a stylized white 'S' composed of horizontal lines to the left of the text 'SEIWA' in a bold, white, sans-serif font, with 'OPTICAL' in a smaller, white, sans-serif font below it.



NEW IR-2200 Microscope

For fast performance and high precision measurements

LEARN MORE 

Nanomechanical probing of thin-film dielectric elastomer transducers

Bekim Osmani,¹ Saman Seifi,² Harold S. Park,² Vanessa Leung,¹ Tino Töpfer,¹ and Bert Müller^{1,a)}

¹*Biomaterials Science Center, Department of Biomedical Engineering, University of Basel, Allschwil 4123, Switzerland*

²*Department of Mechanical Engineering, Boston University, Boston, Massachusetts 02215, USA*

(Received 4 May 2017; accepted 13 August 2017; published online 31 August 2017)

Dielectric elastomer transducers (DETs) have attracted interest as generators, actuators, sensors, and even as self-sensing actuators for applications in medicine, soft robotics, and microfluidics. Their performance crucially depends on the elastic properties of the electrode-elastomer sandwich structure. The compressive displacement of a single-layer DET can be easily measured using atomic force microscopy (AFM) in the contact mode. While polymers used as dielectric elastomers are known to exhibit significant mechanical stiffening for large strains, their mechanical properties when subjected to voltages are not well understood. To examine this effect, we measured the depths of 400 nanoindentations as a function of the applied electric field using a spherical AFM probe with a radius of (522 ± 4) nm. Employing a field as low as $20 \text{ V}/\mu\text{m}$, the indentation depths increased by 42% at a load of 100 nN with respect to the field-free condition, implying an electro-mechanically driven elastic softening of the DET. This at-a-glance surprising experimental result agrees with related nonlinear, dynamic finite element model simulations. Furthermore, the pull-off forces rose from (23.0 ± 0.4) to (49.0 ± 0.7) nN implying a nanoindentation imprint after unloading. This embossing effect is explained by the remaining charges at the indentation site. The root-mean-square roughness of the Au electrode raised by 11% upon increasing the field from zero to $12 \text{ V}/\mu\text{m}$, demonstrating that the electrode's morphology change is an undervalued factor in the fabrication of DET structures. © 2017 Author(s). All article content, except where otherwise noted, is licensed under a Creative Commons Attribution (CC BY) license (<http://creativecommons.org/licenses/by/4.0/>). [<http://dx.doi.org/10.1063/1.5000736>]

Thin-film dielectric elastomer transducers (DETs) are emerging in applications such as haptics, tunable optics, soft robotics, and biomedical devices.¹ In their most primitive version, they are composed of a soft elastomeric film, sandwiched between two compliant electrodes. The elastomer film, often polydimethylsiloxane (PDMS), undergoes an expansion perpendicular to the applied electric field as a result of the Coulomb attraction of the oppositely charged electrodes. DETs show an actuation strain larger than muscles in the human body² and millisecond response time³ and have energy densities well comparable to human muscle tissue.^{4,5} In addition, composed of elastomers,⁶ they can self-heal⁷ and can provide sensing feedback.⁸ Thus, DETs could become medical devices to substitute the function of human muscles.⁹ The generated force of a thin-film DET with an area of about a square-centimeter was found to be 100 mN and could be quantified using an optical beam-deflection technique.¹⁰ Therefore, thousands of layers would be required to generate forces of several Newtons, which is required for artificial muscles to treat urinary or fecal incontinence. A recent work describes the fabrication of a 12-layer stacked DET that allows significant actuations without pre-stretching at voltages between 1 and 2 kV.¹¹ Major efforts have been invested to reduce the operation voltage by one or two orders of magnitude. One approach relies on elastomer films with a submicron thickness which are prepared by thin-

film techniques such as molecular beam deposition (MBD) techniques and electrospraying.^{12,13} The surface roughness of thermally evaporated metal/PDMS sandwich structures can be controlled on the nanometer scale;¹⁴ however, their applicability for DETs is still restricted. First, the evaporation of viscous PDMS pre-polymers in vacuum is limited to oligomers with a molecular weight of 6100 g/mol (Ref. 15); second, the growth rate below one layer per hour confines the fabrication of stacked DETs.¹⁶ Electrospraying of dissolved PDMS in ethyl acetate exhibits increased deposition rates of one layer per minute but leads to comparably rough PDMS sub-micrometer films. However, it is easily scalable and promising for large-scale fabrication of low-voltage DETs. The performance of electrosprayed DETs with inhomogeneous PDMS films has not been investigated yet. Recently, it has been shown that for thin-film DETs, the impact of electrode's topology and stiffness increase of the overall DET by a metal electrode, such as Au, is essential.¹⁷ In a previous study, these mechanical properties have been determined by nanoindentation (NI) measurements with a spherical indenter using atomic force microscopy (AFM).¹⁸ The elastic modulus of the thin-film DET sandwich structure increased by a factor of three after the deposition of a 10 nm Au electrode. The observed force-distance-curves allow us not only to extract the mechanical properties of thin polymeric films but also to study the related adhesion forces.^{19–22} Several research teams have investigated the electromechanical behavior for larger deformations using experimental

^{a)}Author to whom correspondence should be addressed: bert.mueller@unibas.ch

methods and simulations including finite element (FE) analysis.^{23–26}

In this communication, we elucidate that probing a DC-powered thin-film DET with a spherical AFM tip leads to increased indentation depths by several tens of percent, as verified by dynamic FE models. Furthermore, we investigate how far the roughness of the Au electrode increases owing to the actuation. This effect is highly beneficial and can be used in anisotropic DET structures with electrodes containing parallel wrinkles to generate unilateral actuation.

Single-layer DET specimens, as shown in Fig. 1(a), were fabricated on polyethylene naphthalate (PEN) polymeric substrates. The related materials and fabrication methods are presented in a previous work.¹⁰ For the nanoindentation (NI) measurements, the 10 nm-thin Au electrodes were connected to the DC power supply and set to selected voltages between 0 and 160 V. The voltage Φ was set to the preselected value and kept constant until the completion of the 400 NI measurements. For all experiments, we used only one AFM cantilever with a spherical electron-beam processed carbon tip (B500 FMR, Nanotools GmbH, Germany). The tip radius has been measured using scanning electron microscopy and is found to be (522 ± 4) nm. The nominal spring constant of the AFM cantilever was calculated using the Sader method and was found to be $k = (1.9 \pm 0.1)$ N/m. According to the Global Calibration Initiative by Sader *et al.*, we get for this cantilever a standardized spring constant of $k_{\text{Sader}} = (2.1 \pm 0.2)$ N/m ($f_r = 88.9$ kHz, $Q = 132$, B500 FMR).²⁷ The deflection sensitivity was calibrated using a Si wafer serving as a substrate with an infinite stiffness. An area of $10 \times 10 \mu\text{m}^2$ contains 400 subdomains, each serving as a NI site. An automated data acquisition and analysis software (Flex-ANA, Nanosurf AG, Switzerland) running on an AFM system (FlexAFM C3000, Nanosurf AG, Switzerland) was used to extract the indentation depths δ for each measurement. The nanoindentation speed was set to $3 \mu\text{m/s}$. PDMS can be approximated to be purely elastic.²¹ Characteristic force-distance curves for

$P = 100$ nN and $\Phi = 0$ V shown in the [supplementary material](#) clearly indicate that the PDMS-layer shows an almost perfectly elastic behavior as the loading and unloading curve coincide.

NIs on DETs without applying a voltage, $\Phi = 0$ V, were employed to determine the average elastic modulus E_{DET} . The dimensionless Tabor parameter $\mu = (R\gamma^2/E_{\text{DET}}^2\epsilon^3)^{1/3}$ supports selecting the contact model.²⁸ Here, R is the probe radius, γ the adhesion work, and ϵ the equilibrium separation, typically around 0.5 nm. For $\mu > 5$, the Johnson-Kendall-Roberts (JKR) contact model is recommended.^{28,29} Using $R = 522$ nm and the average pull-off force $F_0 = 23$ nN, the adhesion work $\gamma = F_0/(3\pi R/2)$ is found to be 9.3 mJ/m². With $E_{\text{DET}} = 1.6$ MPa, the Tabor parameter can be calculated to be $\mu = 52$. For $\Phi = 0$ V, the experimental data clearly uncover the two-layer DET structure consisting of the 10 nm-thin electrode and the elastomeric bulk. For a small load of $P = 25$ nN, the calculated average elastic modulus using the JKR model corresponds to $E_{\text{DET}} = (2.1 \pm 0.3)$ MPa. It decreases to (1.8 ± 0.2) , (1.7 ± 0.2) , and (1.6 ± 0.2) MPa for loads of $P = 50, 75$, and 100 nN, respectively. The nanoindentation depths for $\Phi = 0$ V are listed in Table I. The elastic modulus decreases with the indentation depth for the two-layer structure. We assume that local strains on the 10 nm-thin Au electrode rise for larger penetration depths minimizing the stiffness increase due to the stiff electrode. It was shown, however, that the surface layer of PDMS is stiffer than the PDMS below.³⁰ As reported previously, the nanometer-thin Au electrode is not confluent and forms nanoclusters with a nominal size of (20 ± 10) nm.³¹ NI results on actuated DETs operated at voltages of $\Phi = 0, 40, 80, 120$, and 160 V are summarized in Table I for applied loads of $P = 25, 50, 75$, and 100 nN. The resulting mean indentation depth δ including the measurements at $\Phi = 0$ V were fitted using a Gaussian function.

For a constant indentation load P , the indentation depth δ increases with respect to the applied voltage Φ . We assume that the indentation depth increases with the applied voltage due to an increased charge density at the indentation site. It is shown that the electric charge density at a point on a given conductor surface increases with its local curvature $1/R$.³² These experimental results were surprising at first glance, as one might expect a stiffening effect due to the applied Maxwell pressure generated.² For $P = 25$ nN, the indentation depth is increased by 17 nm, whereas for $P = 100$ nN, the average increase was found to be 50 nm. The variance of measured data increased as well. The nonlinear, dynamic

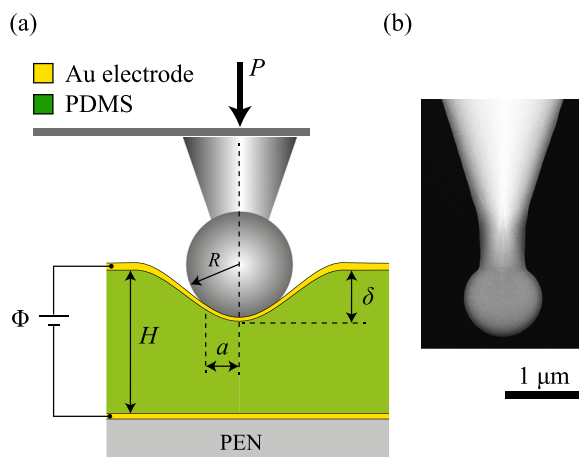


FIG. 1. AFM nanoindentation on the activated DET structure. (a) Schematic of the experimental setup consisting of an $8 \mu\text{m}$ -thin elastomer film, sandwiched between two 10 nm-thin Au electrodes. The nanoindentation depth δ is measured at selected voltages Φ and loads P using an AFM probe with a well-defined radius R . The spherical tip gives rise to the contact radius a used for the JKR model.²⁸ (b) SEM image of the used spherical probe with a radius of (522 ± 4) nm. Reproduced with permission from Nanotools GmbH, Munich, Germany. Copyright 2017 Nanotools GmbH.

TABLE I. Indentation depths δ of a spherical AFM probe on a single-layer thin-film DET at selected loads P and applied voltages Φ . The derived parameters are grouped and fitted using a Gaussian.

Indentation load P (nN)	Indentation depth δ (nm) ^a				
	$\Phi = 0$ V	$\Phi = 40$ V	$\Phi = 80$ V	$\Phi = 120$ V	$\Phi = 160$ V
25	38 ± 4	40 ± 5	46 ± 5	51 ± 5	55 ± 6
50	74 ± 6	75 ± 6	83 ± 8	93 ± 8	114 ± 16
75	103 ± 6	106 ± 7	113 ± 8	125 ± 9	143 ± 11
100	117 ± 4	132 ± 6	140 ± 7	151 ± 8	167 ± 11

^aThe error corresponds to the standard deviation of the Gaussian fit.

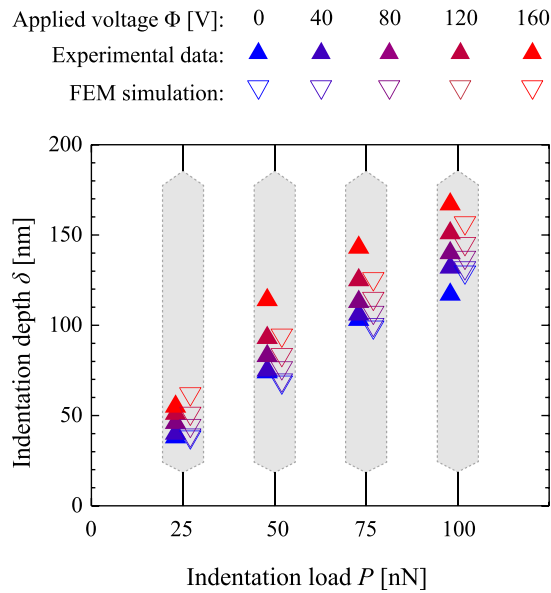


FIG. 2. Indentation depth δ as a function of the applied load P for selected voltages Φ . The FE simulations explain the experimental data.

finite element (FE) simulations, as shown in Fig. 2, agree with the experimental results. The FE simulations were carried out using a previously developed dynamic FE formulation for DETs.³³ 2D plane strain FE simulations were performed on DETs with the same material properties. The voltage at the bottom surface was kept at zero, while the voltage was increased linearly on the top surface in Fig. 1 and the voltage was increased sufficiently slowly to mimic quasi-static loading conditions. After the voltage reached the target value, the DET was indented by moving the indenter towards the DET with fixed velocity. The reaction force as a function of indentation depth was then measured, and the FE simulations were repeated for the voltages, as in the experiments. We have observed that at higher loads P , the experimental data are pulled apart more strongly than the values observed from the FE simulation. The indentation depths δ from FE simulations overshoot the experimental data at smaller voltages and fall below the experimental data at higher voltages Φ . This is likely because the FE models assume “ideal dielectric behavior,” i.e., the polarization of the dielectric is like a fluid or isotropic.

The loading curves of NI experiments include both the contact and adhesion forces. From the unloading force-distance curves, however, the pull-off force F_0 , also termed adhesion force at the time of separation, is extracted. The pull-off force F_0 is given as²⁹

$$F_0 = 2\pi R(\gamma_1 + \gamma_2 - \gamma_{12}), \quad (1)$$

where R is the indenter radius and γ_1 , γ_2 , and γ_{12} are the free surface energies of the indentation sphere, the electrode and the interface, respectively. In Fig. 3, we show the categorized pull-off forces from 400 nanoindentations at a fixed load of $P = 100$ nN. The histograms were consistently fitted using OriginPro 2015 (OriginLab Corporation, Northampton, USA) and pro Fit 6.2.11 (QuantumSoft, Uetikon am See, Switzerland) to one Gaussian with the three relevant parameters including their error bars by means of the Levenberg-Marquardt algorithm.

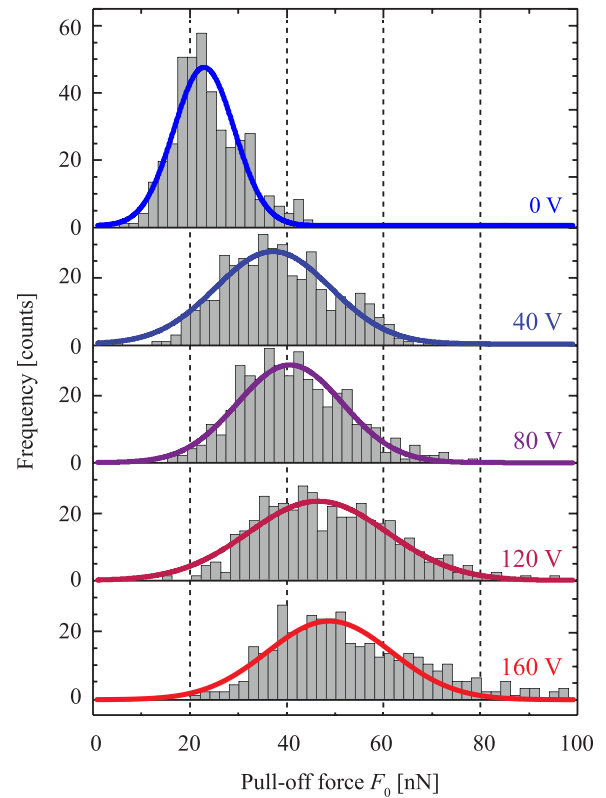


FIG. 3. Histograms of pull-off forces F_0 at the time of separation extracted from the unloading force distance curves for an applied load of $P = 100$ nN. The obtained values are fitted with a Gaussian function, upon which for the mean values we find $F_0 = (23.0 \pm 0.4)$, (37.2 ± 0.6) , (40.7 ± 0.5) , (46.4 ± 0.7) , and (49.0 ± 0.7) nN for $\Phi = 0, 40, 80, 120$, and 160 V, respectively.

We have observed more than a doubling of the pull-off forces from (23.0 ± 0.4) to (49.0 ± 0.7) nN with increased operation voltages from $\Phi = 0$ to 160 V. Equation (1) illustrates the proportionality of pull-off force to the size of the indenter sphere. Therefore, we assume that the increased pull-off forces are related to an increased contact area at the instant of time when the indenter is being separated from the Au electrode. We hypothesize that a *nano-indentation imprint* remains after the measurement due to charge accumulation at the indentation site of the activated DET structure. Although our AFM instrumentation does not allow direct scanning of the topology after indentation, it is a reasonable hypothesis because adhesion measurements on stiff Au-coated Si wafers show that the pull-off forces are independent of the applied load and indentation speed. An electrostatic field between the cantilever and the top gold electrode layer can be excluded as they were connected at a single point to avoid an electrical potential. The related data are given in the [supplementary material](#). As reported by Rabinovich *et al.*, the adhesion forces decrease with respect to the surface roughness.³⁴ Therefore, in the present experiment, one can definitely exclude any increase in the adhesion force as a result of enhanced surface roughness. However, doubling the applied voltage Φ from 80 to 160 V, the pull-off force F_0 only increases by 20%, i.e., from (40.7 ± 0.5) to (49.0 ± 0.7) nN.

Figure 4 shows AFM surface scans of planar electrodes for $\Phi = 0$ and 100 V. The scans were performed in the tapping mode (Budget Sensors Tap 190-G, Nano and More GmbH, Wetzlar, Germany) with an amplitude of 1 V and a

set point of 60%. The typical Volmer-Weber growth mode of Au on PDMS leads to nanoclusters with an average size of (20 ± 10) nm. At applied voltages of 100 V, the detected surface roughness increased by 11%. The charge distribution on the electrode of a powered DET is expected to be strongly dependent on the topology of the electrode. Due to charge accumulation within the valleys, the electric field becomes inhomogeneous on the nanometer scale. This effect could be related to the indentation depth, which increases with the voltage applied, as elucidated by the experimental data shown in Fig. 2.

As recently published, we were able to follow the compressive strain of a DET structure using the AFM in real time.³⁵ For this, the upper electrode was scanned in the contact mode with a comparably soft spherical AFM tip (B150 CONTR, $k=0.2$ N/m) at the low set point of 8 nN to minimize the penetration of the tip into the DET structure. The calculated contact pressure was found to be 0.48 MPa. The radius of the AFM tip was measured using scanning electron microscopy and was found to be $R=(152 \pm 2)$ nm. To ensure a verifiable contact between the AFM tip and the electrode, we have fabricated DET structures with parallel aligned wrinkles as seen in Fig. 5(a). DET structures were fabricated on 2-in. Si substrates with a 100 nm SiO₂ coating using a Mo mask with 12×0.4 mm² windows. As Bowden *et al.* have shown, wrinkles align perpendicular to steps and edges.³⁶ Due to the oriented wrinkle structure over the whole width, at one end of the DET, the upper electrode was displaced by $s_x=(80 \pm 3)$ μ m in one direction, as observed with the built-in top camera of the AFM system. The compressive strain was extracted via two profile cuts as seen in Fig. 5(b). The profile cuts were fitted using a constant revealing an actuation of (180 ± 20) nm. This value corresponds to a strain of only 2.3%, as the DET structure was fabricated on a rigid Si wafer. The calculated RMS value for $\Phi=0$ V and $\Phi=100$ V of the AFM scan shown in Fig. 5(b) increased from 23 to 28 nm.

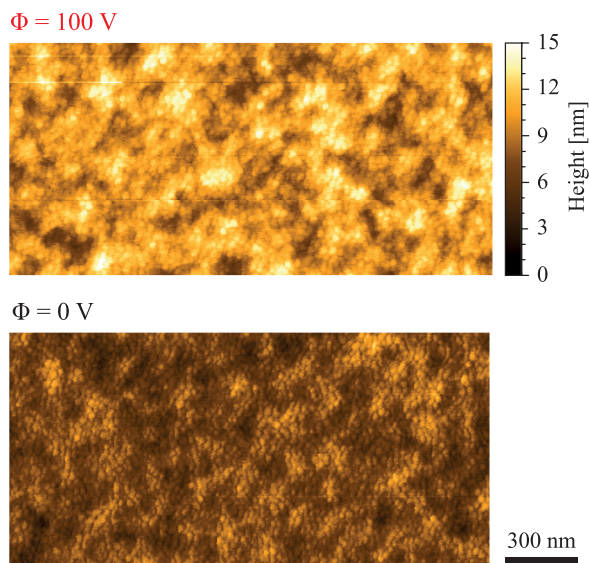


FIG. 4. AFM surface scan of a 2×1 μ m² spot of the top Au electrode for a non-powered and powered DET. For a voltage of $\Phi=100$ V, which corresponds to an electric field of 12 V/ μ m, the root-mean-square roughness increased by 11%, from 1.35 to 1.50 nm. The height color bar is valid for both AFM scans.

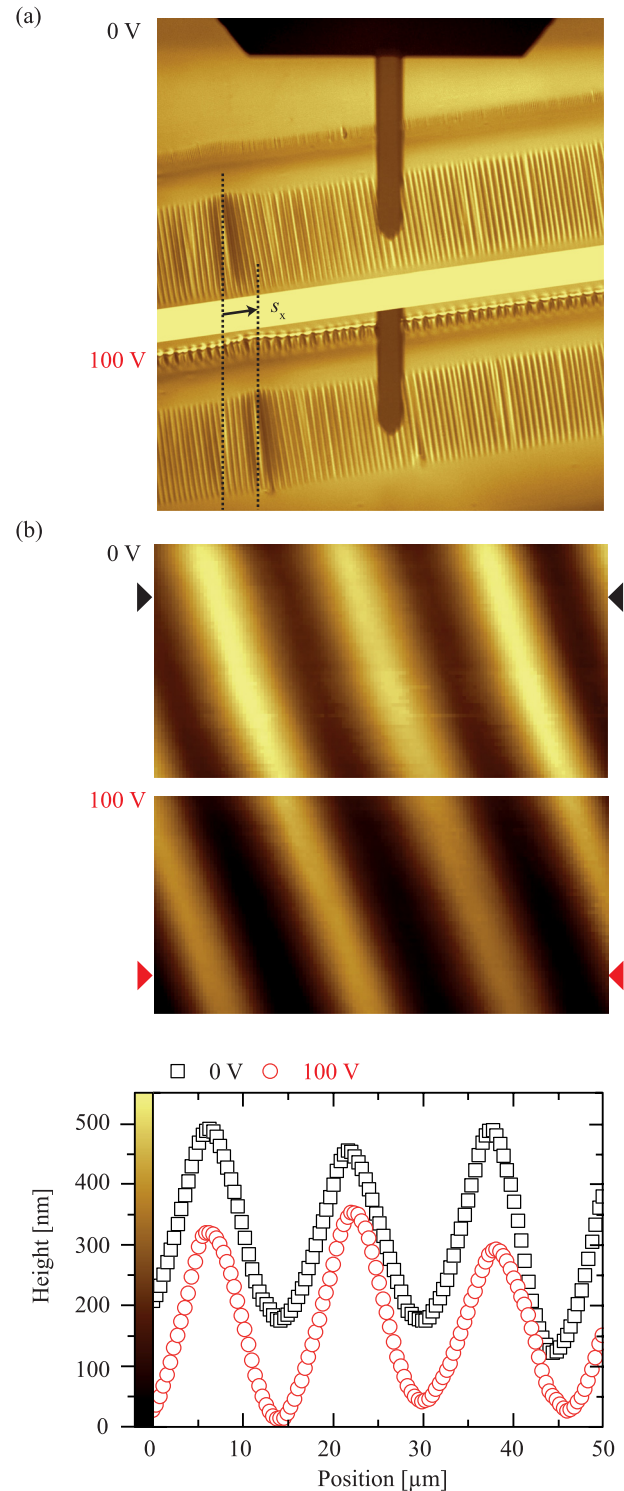


FIG. 5. Actuation measurement of a substrate bonded single-layer DET using an AFM in the contact mode. (a) Observation of the lateral displacement $s_x=(80 \pm 3)$ μ m of the wrinkled electrode using the built-in top camera of the AFM. (b) AFM scan in the contact mode of the wrinkled electrode using a spherical AFM tip with a large radius of $R=(152 \pm 2)$ nm for $\Phi=0$ and 100 V. Profile cuts reveal a compressive actuation of only (180 ± 20) nm, corresponding to a strain of only 2.3%, as the DET structure was fabricated on a rigid Si wafer. The height color bar for the AFM scans is shown on the left side/ordinate of the graph containing the profile cuts.

In summary, we have shown that probing a DC-powered thin-film DET with an AFM spherical tip leads to increased indentation depths by several tens of percent, as verified by dynamic FE models. We address the apparent softening

effect of the DET structure as a result of the expected charge accumulation at the nanoindentation site, which is the consequence of the impression by the tip.³² Furthermore, AFM scans revealed increased roughness of the Au electrode as a result of the voltage applied to the DET. In conclusion, electrodes with a controlled topology can be prepared to trigger a preferred direction of the actuation.

See [supplementary material](#) for details on the sample preparation, characteristic force-distance curves, average elastic modulus using the JKR contact model for the DET-structure at four selected loads, and pull-off forces for a spherical AFM tip with a radius of (499 ± 4) nm on a 50 nm-thin Au-coated Si wafer.

This work was conducted with financial support from the Swiss Research Program Nano-Tera.ch as well as from the Swiss Nanoscience Institute (SNI). HSP and SS acknowledge funding from the ARO, grant W911NF-14-1-0022.

- ¹S. Rosset and H. R. Shea, *Appl. Phys. Rev.* **3**(3), 031105 (2016).
- ²R. Pelrine, R. Kornbluh, Q. Pei, and J. Joseph, *Science* **287**(5454), 836 (2000).
- ³J. Kun, L. Tongqing, and T. J. Wang, *Sens. Actuators, A* **239**, 8 (2016).
- ⁴A. O'Halloran, F. O'Malley, and P. McHugh, *J. Appl. Phys.* **104**(7), 071101 (2008).
- ⁵I. A. Anderson, T. A. Gisby, T. G. McKay, B. M. O'Brien, and E. P. Calius, *J. Appl. Phys.* **112**(4), 041101 (2012).
- ⁶D. Rus and M. T. Tolley, *Nature* **521**(7553), 467 (2015).
- ⁷S. Hunt, T. G. McKay, and I. A. Anderson, *Appl. Phys. Lett.* **104**(11), 113701 (2014).
- ⁸G. Rizzello, D. Naso, A. York, and S. Seelecke, *Smart Mater. Struct.* **25**(3), 035034 (2016).
- ⁹E. Fattorini, T. Brusa, C. Gingert, S. E. Hieber, V. Leung, B. Osmani, M. D. Dominietto, P. Büchler, F. Hetzer, and B. Müller, *Ann. Biomed. Eng.* **44**, 1355 (2016).
- ¹⁰B. Osmani, E. A. Aeby, and B. Müller, *Rev. Sci. Instrum.* **87**(5), 053901 (2016).

- ¹¹M. Duduta, R. J. Wood, and D. R. Clarke, *Adv. Mater.* **28**(36), 8058 (2016).
- ¹²F. M. Weiss, T. Töpfer, B. Osmani, H. Deyhle, G. Kovacs, and B. Müller, *Langmuir* **32**, 3276 (2016).
- ¹³T. Töpfer, F. M. Weiss, B. Osmani, C. Bippes, V. Leung, and B. Müller, *Sens. Actuators, A* **233**, 32 (2015).
- ¹⁴T. Töpfer, S. Lörcher, H. Deyhle, B. Osmani, V. Leung, T. Pfohl, and B. Müller, *Adv. Electron. Mater.* **3**, 1700073 (2017).
- ¹⁵T. Töpfer, S. Lörcher, F. Weiss, and B. Müller, *APL Mater.* **4**(5), 56101 (2016).
- ¹⁶F. M. Weiss, T. Töpfer, B. Osmani, S. Peters, G. Kovacs, and B. Müller, *Adv. Electron. Mater.* **2**, 1500476 (2016).
- ¹⁷A. Poulin, S. Rosset, and H. R. Shea, *Appl. Phys. Lett.* **107**(24), 244104 (2015).
- ¹⁸B. Osmani, H. Deyhle, F. M. Weiss, T. Töpfer, M. Karapetkova, V. Leung, and B. Müller, *Proc. SPIE* **9798**, 979822 (2016).
- ¹⁹K. Miyake, N. Satomi, and S. Sasaki, *Appl. Phys. Lett.* **89**(3), 031925 (2006).
- ²⁰M. Galli and M. L. Oyen, *Appl. Phys. Lett.* **93**(3), 031911 (2008).
- ²¹F. Carrillo, S. Gupta, M. Balooch, S. J. Marshall, G. W. Marshall, L. Pruitt, and C. M. Puttlitz, *J. Mater. Res.* **20**(10), 2820 (2005).
- ²²H. J. Butt, B. Cappella, and M. Kappl, *Surf. Sci. Rep.* **59**(1), 1 (2005).
- ²³M. Wissler and E. Mazza, *Sens. Actuators, A* **138**(2), 384 (2007).
- ²⁴S. Seifi and H. S. Park, *Int. J. Solids Struct.* **87**, 236 (2016).
- ²⁵H. S. Park, Z. Suo, J. Zhou, and P. A. Klein, *Int. J. Solids Struct.* **49**(15–16), 2187 (2012).
- ²⁶X. Zhao and Q. Wang, *Appl. Phys. Rev.* **1**(2), 021304 (2014).
- ²⁷J. E. Sader, R. Borgani, C. T. Gibson, D. B. Haviland, M. J. Higgins, J. I. Kilpatrick, J. Lu, P. Mulvaney, C. J. Shearer, A. D. Slattery, P. A. Thorén, J. Tran, H. Zhang, H. Zhang, and T. Zheng, *Rev. Sci. Instrum.* **87**(9), 093711 (2016).
- ²⁸Yu. M. Efremov, D. V. Bagrov, M. P. Kirpichnikov, and K. V. Shaitan, *Colloids Surf., B* **134**, 131 (2015).
- ²⁹D. Tabor, *J. Colloid Interface Sci.* **58**(1), 2 (1977).
- ³⁰W. Xu, N. Chahine, and T. Sulchek, *Langmuir* **27**(13), 8470 (2011).
- ³¹B. Osmani, T. Töpfer, M. Siketanc, G. Kovacs, and B. Müller, *Proc. SPIE* **10163**, 101631E (2017).
- ³²K. Bhattacharya, *Phys. Scr.* **91**(3), 035501 (2016).
- ³³H. S. Park, Q. Wang, X. Zhao, and P. A. Klein, *Comput. Methods Appl. Mech. Eng.* **260**, 40 (2013).
- ³⁴Y. I. Rabinovich, J. J. Adler, A. Ata, R. K. Singh, and B. M. Moudgil, *J. Colloid Interface Sci.* **232**(1), 17 (2000).
- ³⁵T. Töpfer, B. Osmani, S. Lörcher, and B. Müller, *Proc. SPIE* **10163**, 101631F (2017).
- ³⁶N. Bowden, W. T. S. Huck, K. E. Paul, and G. M. Whitesides, *Appl. Phys. Lett.* **75**(17), 2557 (1999).